Quasi-physical phase compensation in digital holographic microscopy

Qu, Weijuan; Choo, Chee Oi; Singh, Vijay Raj; Yu, Yingjie; Anand, Asundi

2009

Qu, W., Choo, C. O., Singh, V. R., Yu, Y., & Anand, A. (2009). Quasi-physical phase compensation in digital holographic microscopy. Journal of the Optical Society of America, 26(9), 2005-2011.

https://hdl.handle.net/10356/93754

https://doi.org/10.1364/JOSAA.26.002005

Quasi-physical phase compensation in digital holographic microscopy

Weijuan Qu,[1,*] Chee Oi Choo,[1] Vijay Raj Singh,[2] Yu Yingjie,[3] and Anand Asundi[2]

[1]*Ngee Ann Centre of Innovation (NACOI), Ngee Ann Polytechnic, 535 Clementi Road, Singapore 599489*
[2]*School of Mechanical and Aerospace Engineering, Nanyang Technological University, 50 Nanyang Avenue, Singapore 639798*
[3]*Department of Precision Mechanical Engineering, Shanghai University, No. 149 Yanchang Road, Shanghai, China 200072*
[*]*Corresponding author: qwe2@np.edu.sg*

Received March 24, 2009; revised July 2, 2009; accepted July 22, 2009;
posted July 24, 2009 (Doc. ID 109186); published August 20, 2009

In digital holographic microscopy, if an optical setup is well aligned, the phase curvature introduced by the microscope objective (MO) together with the illuminating wave to the object wave is a spherical phase curvature. It can be physically compensated by introducing the same spherical phase curvature in the reference beam. Digital holographic microscopy setups based on the Michelson interferometric configuration with MO and an adjustable lens are presented, which can well perform the quasi-physical phase compensation during the hologram recording. In the reflection mode, the adjustable lens serves as both the condensing lens and the compensation lens. When the spatial frequency spectra of the hologram become a point spectrum, one can see that the phase curvature introduced by imaging is quasi-physically compensated. A simple plane numerical reference wavefront used for the reconstruction can give the correct quantitative phase map of the test object. A theoretical analysis and experimental demonstration are given. The simplicity of the presented setup makes it easy to align it well at lower cost.

OCIS codes: 090.1995, 180.0180, 120.3620.

1. INTRODUCTION

In general, digital holographic microscopy (DHM) can be achieved in two ways. One is using spherical diverging waves [1,2] for the hologram recording, which allows an enlargement of the object by reconstructing a magnified hologram during the numerical reconstruction process with a collimated plane reference wave without any image-forming lens. The other way is using a microscope objective (MO) [3–5]. The MO in DHM can give microscopic imaging of the test sample with axial nanometric accuracy. It has found many applications in material and life science [6,7] as a result of the quantitative phase measurement. Nevertheless, both the spherical illuminating wave and the MO will introduce phase curvature in the object wave, which should be compensated by a numerical phase mask [5,8–12] or by physically introducing the same curvature in the reference wave [2–4,13,14].

In numerical compensation, a correct numerical reference wave together with a phase mask is needed to fulfill the task of acquiring the quantitative phase in the reconstruction process [5,8]. The reconstructed wavefront multiplies the digital phase mask (DPM), which is a complex-numbers array and can be automatically computed [11], to remove the additional phase curvature coming from either the illumination wavefront or the MO. Usually the definition and the position of the DPM used to compensate the phase curvature are very different [12]. In the case of compensation in the reconstruction plane, the phase mask has to be adapted when the reconstruction distance is changed. This complicates the reconstruction algorithm and requires a calibration procedure, which makes the numerical reconstruction a time-consuming process. This may lead to failure of the real-time monitoring of the test specimen.

One also can physically introduce the same curvature in the reference wave, such as the Linnik interferometer [14] or the Mach–Zehnder configuration [3,4,13]. In this configuration the use of the measurement optics in the reference arm duplicates the objective measurement optics in the measurement arm. So curvature of the object wave is then compensated by the reference wave during interference. Nevertheless, it requires a precise alignment of all the involved optical elements.

As the use of MO only in the object beam introduces a spherical phase curvature [12], a spherical wavefront in the reference beam may provide quasi-physical phase compensation if the adjustable lens is properly located [15]. In this paper, we propose both the reflection-mode and the transmission-mode DHM based on the Michelson interferometric configuration with MO and an adjustable lens, which gives quasi-physical phase compensation in the recording process of the digital hologram. In Section 2, theoretical analysis of the two spherical wavefronts interference is given. In Section 3, the experimental setup of the proposed transmission-mode and reflection-mode DHM is described. In Section 4, an experimental demonstration of the quasi-physical phase compensation is given.

2. BASES OF DIGITAL HOLOGRAPHY

A. Hologram Recording

Digital holography consists of recording a digitized hologram by using an electronic device [e.g., a charge coupled device (CCD)] and later reconstructing the hologram numerically with a computer. In this process, both the amplitude and the phase of an optical wave arrive from a coherently illuminated object. Thus, both hardware and software are needed in digital holography. A digital hologram is created by interference; that is, an unknown wavefront coming from the object, called object wave O, is added to the reference wave R to give an intensity modulated by the phases of the two waves. The intensity $I_H(x,y)$ of the sum of two complex fields can be written as

$$I_H(x,y) = |O+R|^2 = |O|^2 + |R|^2 + RO^* + R^*O, \qquad (1)$$

where RO^* and R^*O are the interference terms with R^* and O^* denoting the complex conjugate of the two waves.

The digital hologram reconstruction is achieved by illumination with a numerical reference wave C. The reconstructed wavefront in the hologram plane is then given by

$$\psi(x,y) = C(|O|^2 + |R|^2) + CRO^* + CR^*O. \qquad (2)$$

For in-line recording geometry, the zero-order and the twin images are superposed on one another. It is hard to separate the object information of interest from one single hologram, which is limited in application in real-time inspection. For off-axis recording geometry, the separation of the three terms enables further operation of the digital hologram, such as apodization and spatial filtering [16]. After that, the terms necessary to reproduce the original wavefront $\psi^H(x,y)=CR^*O$ in the hologram plane are achieved and are propagated to the image plane, where a focused image $\psi^I(x,y)$ is created.

B. Numerical Reconstruction Algorithms

Two different numerical reconstruction algorithms are used to calculate the scalar diffraction between ψ^H and ψ^I: the single Fresnel transform formulation [12] in the spatial domain and the angular spectrum method in the spatial frequency domain.

Numerical reconstruction of ψ^H by the angular spectrum method requires a Fourier transform and an inverse Fourier transform:

$$\psi^I(n\Delta x_i, m\Delta y_i) = \frac{\exp(\mathrm{j}kd)}{\mathrm{j}\lambda d}\mathrm{FFT}^{-1}\{\mathrm{FFT}\{\psi^H(n\Delta x_H, m\Delta y_H)\} \times G(n\Delta\xi, m\Delta\eta)\},$$

$$G(n\Delta\xi, m\Delta\eta) = \exp\left[\mathrm{j}\frac{2\pi d}{\lambda}\sqrt{1-(\lambda n\Delta\xi)^2-(\lambda m\Delta\eta)^2}\right], \qquad (3)$$

where n and m are integers ($-M/2 \le n \le M/2, -N/2 \le m \le N/2$, and $M\times N$ is the number of pixels of the CCD), $G(n\Delta\xi, m\Delta\eta)$ is the optical transfer function in the spatial frequency domain, $\Delta\xi$ and $\Delta\eta$ are the sampling intervals in the spatial frequency domain, Δx_H and Δy_H are the sampling intervals in the hologram plane (the pixel size of the CCD camera), and Δx_i and Δy_i are the sampling intervals in the image plane. The relation between the sampling intervals of the hologram plane and those of the image plane is $\Delta x_i = 1/(N\Delta\xi) = \Delta x_\mathrm{H}$ and $\Delta y_i = 1/(M\Delta\eta) = \Delta y_\mathrm{H}$.

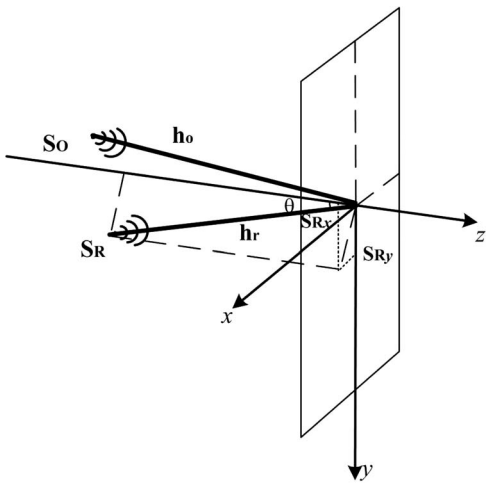

Fig. 1. Schematic of the location of the two point sources.

Both the single Fresnel transform formulation and the angular spectrum method can give correct reconstruction of the recorded hologram. The difference between the two methods is that the single Fresnel transform formulation works in the spatial domain, while the angular spectrum method works in the spatial frequency domain. As the preprocessing of the digital hologram by apodization and spatial filtering involves its Fourier spectra, the angular spectrum method will provide a more time-saving numerical reconstruction of the recorded digital hologram.

C. Theoretical Analysis of Interference between Two Spherical Wavefronts

As the spherical phase curvature involved in the interference in DHM can be totally physically compensated only by a spherical reference wavefront, we now give a theoretical analysis of interference between two spherical wavefronts.

We assumed that the reference wave is generated by a point source located at coordinates $[S_{Rx}, S_{Ry}, (h_r^2 - S_{Rx}^2 - S_{Ry}^2)^{1/2}]$ and the object wave is generated by a point source located at coordinates $[S_{Ox}, S_{Oy}, (h_o^2 - S_{Ox}^2 - S_{Oy}^2)^{1/2}]$, where h_r and h_o are, respectively, the distance between the source points of the reference and object waves and the recombining location of the two beams, as shown in Fig. 1. Using quadratic-phase approximations to the spherical waves involved, the reference wavefront in the hologram plane is thus given by

$$R(x,y) = \exp\left\{-\mathrm{j}\frac{\pi}{\lambda h_r}[(x-S_{Rx})^2 + (y-S_{Ry})^2]\right\}. \qquad (4)$$

The illuminating wave is modulated by the amplitude and phase of the object. In the hologram plane it is given by

$$O(x,y) = A_O \exp\left\{-\mathrm{j}\frac{\pi}{\lambda h_o}[(x-S_{Ox})^2 + (y-S_{Oy})^2]\right\} \times \exp[\mathrm{j}\varphi(x,y)], \qquad (5)$$

where A_O is the amplitude and $\varphi(x,y)$ is the phase intro-

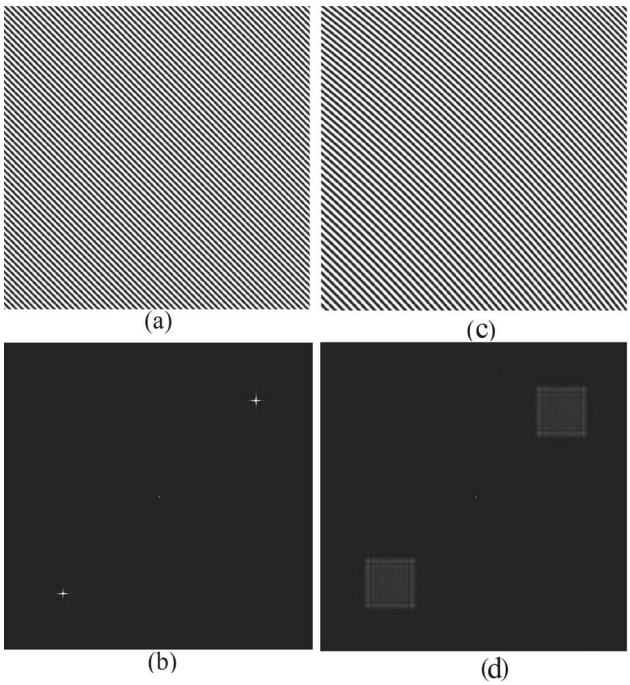

Fig. 2. Spectrum analysis of holograms with different fringe patterns. (a) Hologram with straight fringe pattern. (b) Fourier spectra of hologram (a). (c) Hologram with circular fringe pattern. (d) Fourier spectra of hologram (c).

duced by the test object. The corresponding intensity distribution in the pattern of the interference between the two waves is

$$
\begin{aligned}
I_H(x,y) &= |O|^2 + |R|^2 + RO^* + R^*O \\
&= 1 + |A_O|^2 + A_O \exp\left[-\mathrm{j}\frac{\pi}{\lambda}\left(\frac{S_{Rx}^2}{h_r} - \frac{S_{Ox}^2}{h_o} + \frac{S_{Ry}^2}{h_r} - \frac{S_{Oy}^2}{h_o}\right)\right]\exp\left[-\mathrm{j}\frac{\pi}{\lambda}\left(\frac{1}{h_r} - \frac{1}{h_o}\right)(x^2+y^2) + \mathrm{j}\frac{2\pi}{\lambda}\left(\frac{S_{Rx}}{h_r} - \frac{S_{Ox}}{h_o}\right)x + \mathrm{j}\frac{2\pi}{\lambda}\left(\frac{S_{Ry}}{h_r} - \frac{S_{oy}}{h_o}\right)y\right]\exp[-\mathrm{j}\varphi(x,y)] \\
&\quad + A_O \exp\left[\mathrm{j}\frac{\pi}{\lambda}\left(\frac{S_{Rx}^2}{h_r} - \frac{S_{Ox}^2}{h_o} + \frac{S_{Ry}^2}{h_r} - \frac{S_{Oy}^2}{h_o}\right)\right] \\
&\quad \times \exp\left[\mathrm{j}\frac{\pi}{\lambda}\left(\frac{1}{h_r} - \frac{1}{h_o}\right)(x^2+y^2) - \mathrm{j}\frac{2\pi}{\lambda h_r}\left(\frac{S_{Rx}}{h_r} - \frac{S_{Ox}}{h_o}\right)x - \mathrm{j}\frac{2\pi}{\lambda h_r}\left(\frac{S_{Ry}}{h_r} - \frac{S_{oy}}{h_o}\right)y\right]\exp[\mathrm{j}\varphi(x,y)]. \qquad (6)
\end{aligned}
$$

The items in Eq. (6) are combinations of a spherical wavefront, tilt in the x direction, tilt in the y direction, and a constant phase.

When $h_r = h_o$, the spherical wavefront disappears and leaves only the tilt and the constant phase. This means that the spherical wavefront coming from the illuminating wavefront or the imaging MO is totally physical compensated by the reference wavefront during interference. The pattern of the hologram is a set of cosine fringes

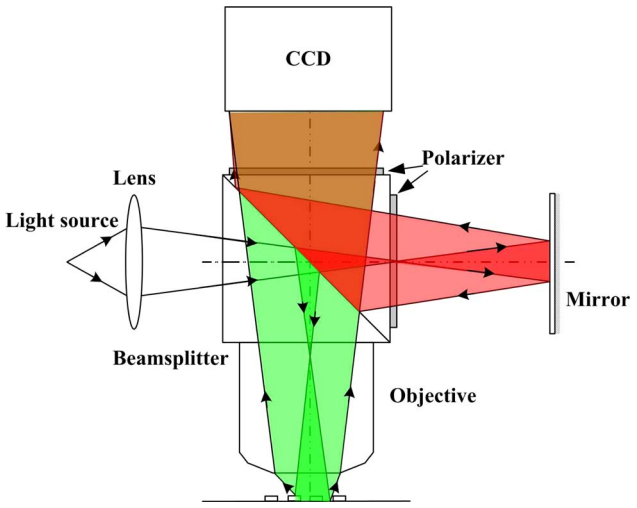

Fig. 3. (Color online) Schematic of the reflection-mode DHM setup.

(straight fringes) which is described by the following equation [as shown in Fig. 2(a)]:

$$
\begin{aligned}
I_H(x,y) &= |O|^2 + |R|^2 + RO^* + R^*O \\
&= 1 + |A_O|^2 + A_O \exp\left[-\mathrm{j}\frac{\pi}{\lambda}\left(\frac{S_{Rx}^2 - S_{Ox}^2 + S_{Ry}^2 - S_{Oy}^2}{h_r}\right)\right] \\
&\quad \times \exp\left[\mathrm{j}\frac{2\pi}{\lambda}\left(\frac{S_{Rx} - S_{Ox}}{h_r}\right)x + \mathrm{j}\frac{2\pi}{\lambda}\left(\frac{S_{Ry} - S_{Oy}}{h_r}\right)y\right]\exp[-\mathrm{j}\varphi(x,y)] \\
&\quad + A_O \exp\left[\mathrm{j}\frac{\pi}{\lambda}\left(\frac{S_{Rx}^2 - S_{Ox}^2 + S_{Ry}^2 - S_{Oy}^2}{h_r}\right)\right] \\
&\quad \times \exp\left[-\mathrm{j}\frac{2\pi}{\lambda h_r}\left(\frac{S_{Rx} - S_{Ox}}{h_r}\right)y - \mathrm{j}\frac{2\pi}{\lambda h_r}\left(\frac{S_{Ry} - S_{Oy}}{h_r}\right)y\right]\exp[\mathrm{j}\varphi(x,y)]. \qquad (7)
\end{aligned}
$$

Its Fourier transform gives the Fourier spectra as three points as shown in Fig. 2(b):

$$
\begin{aligned}
I_H^F(f_x,f_y) &= \delta(f_x,f_y) + \delta\left(f_x - \frac{S_{Rx} - S_{Ox}}{\lambda h_r}, f_y - \frac{S_{Ry} - S_{Oy}}{\lambda h_r}\right) \\
&\quad \otimes \mathrm{FFT}\{\exp[\mathrm{j}\varphi(x,y)]\} \\
&\quad + \delta\left(f_x + \frac{S_{Rx} - S_{Ox}}{\lambda h_r}, f_y + \frac{S_{Ry} - S_{Oy}}{\lambda h_r}\right) \\
&\quad \otimes \mathrm{FFT}\{\exp[-\mathrm{j}\varphi(x,y)]\}. \qquad (8)
\end{aligned}
$$

If there is no test object, the spectra will be a delta function with sharp point distribution. When an object is tested, the convolution in Eq. (8) will make the sharp point distribution a little smoother. However, one still can find a maximum point in each of the spectra, which will help to fulfill the further operation of the digital hologram, such as apodization and spatial filtering.

Note that here we do not mention use of the numerical reference wavefront. Actually, it is a plane numerical reference wavefront without introducing any additional phase to the reconstructed object phase.

When $h_r \neq h_o$, the remaining spherical wavefront can be either a diverging one or a converging one, depending on the relative position of the two point sources. This means that the spherical wavefront coming from the illuminating wavefront or the imaging MO cannot be physically compensated by the reference wavefront during interference. The pattern of the hologram is a set of unclosed circular fringes as shown in Fig. 2(c). The off-axis value is so large that the fringe pattern seems the same as that of Fig. 2(a). The difference can be told by the fringe pattern's Fourier spectra. Its Fourier transform gives the Fourier spectra distribution as shown in Fig. 2(d),

$$
\begin{aligned}
I_H^F(f_x,f_y) = \delta(f_x,f_y) + \mathrm{j}\lambda\frac{h_r h_o}{h_o - h_r}\exp\left[\mathrm{j}\pi\lambda\frac{h_r h_o}{h_o - h_r}(f_x^2 + f_y^2)\right] \\
\otimes \delta\left(f_x - \frac{S_{Rx} - S_{Ox}}{\lambda h_r}, f_y - \frac{S_{Ry} - S_{Oy}}{\lambda h_r}\right) \\
\otimes \mathrm{FFT}\{\exp[\mathrm{j}\varphi(x,y)]\} + \mathrm{j}\lambda\frac{h_r h_o}{h_o - h_r} \\
\times \exp\left[-\mathrm{j}\pi\lambda\frac{h_r h_o}{h_o - h_r}(f_x^2 + f_y^2)\right] \\
\otimes \delta\left(f_x + \frac{S_{Rx} - S_{Ox}}{\lambda h_r}, f_y + \frac{S_{Ry} - S_{Oy}}{\lambda h_r}\right) \\
\otimes \mathrm{FFT}\{\exp[-\mathrm{j}\varphi(x,y)]\}. \qquad (9)
\end{aligned}
$$

The plane numerical reference wavefront is used, so one can see that no additional phase has been introduced to the zero order. But for the plus order and minus order, there are still spherical phase curvatures, indicated by the square spectrum.

Hence the shape of the spectrum can indicate whether the additional phase curvature can be physically compensated during hologram recording. The numerical reference wavefront should be carefully chosen to ensure that no other phase factor is introduced in the reconstructed object phase. One can monitor the shape of the spectrum to judge whether the spherical phase curvature is totally compensated in the setup alignment process.

3. EXPERIMENTAL SETUP

Based on the analysis above, we propose the reflection-mode and the-transmission mode DHM setup based on the Michelson interferometric configuration with MO and an adjustable lens as shown in Figs. 3 and 4.

In the reflection-mode DHM setup, an adjustable lens is inserted in front of the light source (light emitting from a fiber point). The adjustable lens also serves as the condenser of the MO. Thus it will affect both the object beam and reference beam. For the object beam, the lens's position will change the illuminating wavefront and further change the phase curvature produced by the MO. For the reference beam, the mirror reflection adds the propagation distance and then changes its curvature. By adjusting the position of the reflection mirror, one can find a position for the adjustable lens to ensure that both the object beam and the reference beam reach the CCD with the same spherical curvature.

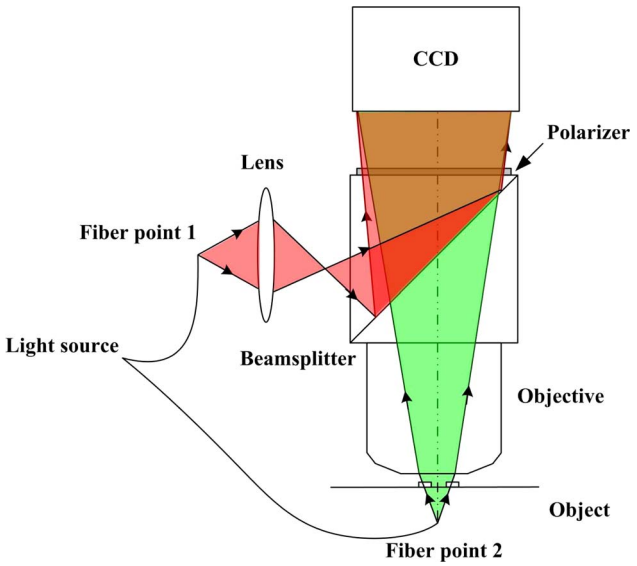

Fig. 4. (Color online) Schematic of transmission-mode DHM setup.

In the transmission mode, the light source is separated into two parts by a fiber coupler to produce the object beam and the reference beam. In the object beam, the location of the light source is carefully chosen to match the numerical aperture of the MO used. In the reference beam, an adjustable lens is used for the phase curvature control to ensure that the reference beam reaches the CCD with the same spherical phase curvature as the object wavefront.

4. EXPERIMENTAL DEMONSTRATION

A sample consisting of a glass substrate with a microscopic laser-ablated spot was investigated in the transmission-mode digital holography setup. The specimen is placed between the light source and the MO. In the reference beam, the adjustable lens is tuned at three different positions to demonstrate the phase curvature compensation. The first position of the adjustable lens is $h_o > h_r$, the second position is $h_o = h_r$, and the third position is $h_o < h_r$. (Actually, h_r and h_o are difficult to measure and quantify in the experiment, but the relation between them can be indicated by the Fourier spectra of the recorded digital hologram, which will be illustrated in what follows.) A 1280×960 pixel CCD with 4.65-μm-square pixels is used to record the digital holograms. The recorded digital holograms are reconstructed by using the angular spectrum method to give the intensity and phase-contrast images of the object.

A plane numerical reference wavefront without any additional phase introduced in the reconstructed object phase is used in the reconstruction process. The Fourier spectra in the frequency domain of each recorded digital

hologram are shown in Fig. 5. For comparison, magnified 3D distributions of the selected plus-order spectrum are given.

When $h_o > h_r$, the spectrum is the convolution among the Fourier spectra of a diverging spherical wavefront, the delta function, and the Fourier transform of the test phase, as shown in Fig. 5(b). The fluctuating boundary of the spectrum indicates the effect of the spherical wavefront, which means that there will be a diverging spherical phase curvature in the reconstructed object phase as shown in Figs. 6(a) and 6(b).

The spectrum for $h_o = h_r$ is shown in Fig. 5(d). It is a kind of point spectrum that has a maximum value among the whole distribution. The phase obtained from this spectrum is shown in Figs. 6(c) and 6(d). There is almost no spherical phase curvature in the reconstructed object phase, which means that the spherical phase curvature introduced by the illuminating wavefront or MO is physically compensated by the reference wavefront during the interference.

When $h_o < h_r$, again the fluctuating boundary is observed in the spectrum shown in Fig. 5(f). It comes from the remaining converging spherical phase curvature. The phase obtained from this spectrum is shown in Figs. 6(e) and 6(f), where a converging spherical phase can be clearly observed.

5. DISCUSSION

If we use the original-recording spherical reference wavefront to reconstruct the hologram shown in Fig. 2, we will obtain a Fourier spectra distribution as shown in Fig. 7.

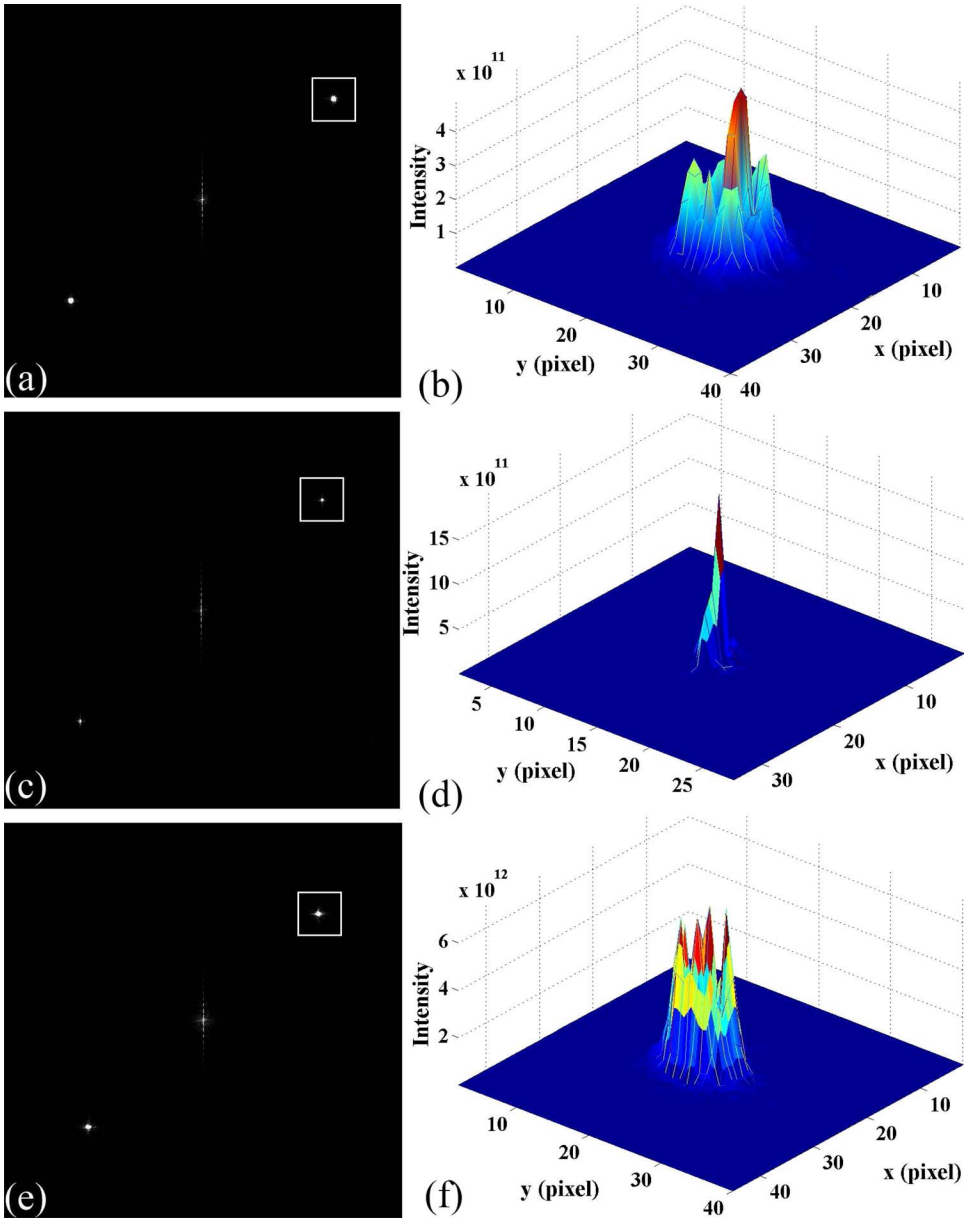

Fig. 5. (Color online) Fourier spectra in the frequency domain. (a) When $h_o > h_r$, Fourier spectra of the recording hologram. (b) Spectrum of the plus order with rectangular shape. (c) Fourier spectra of the recording hologram when $h_o = h_r$. (d) Spectrum of the plus order with point shape. (e) Fourier spectra of the recording hologram when $h_o < h_r$. (f) Spectrum of the plus order with rectangular shape.

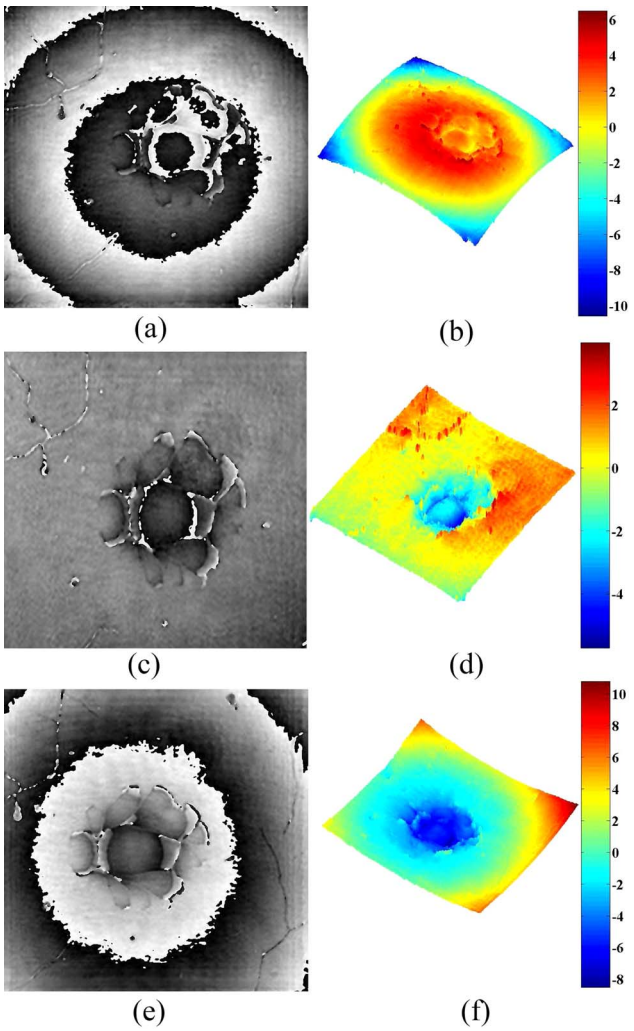

Fig. 6. (Color online) Physical phase compensation demonstration. (a) when $h_o > h_r$, a diverging spherical phase remains. (b) Unwrapped 3D phase map of (a). (c) when $h_o = h_r$, the spherical phase is totally compensated. (d) Unwrapped 3D phase map of (c). (e) when $h_o < h_r$, a converging spherical phase remains. (f) Unwrapped 3D phase map of (e).

Both the plus order and the minus order introduce an additional spherical phase curvature coming from the numerical-reconstruction reference wavefront. For Fig. 7(a), the plus-order spectrum is the convolution between the Fourier spectrum of the numerical spherical reference wavefront and the delta function. For Fig. 7(b), the plus-order spectrum is the convolution among the Fourier spectra of the numerical spherical reference wavefront, the remaining uncompensated spherical wavefront, and the delta function. The phase reconstructed from these spectra by using the angular spectrum method will always contain a spherical phase curvature needing to be numerical compensated by an additional digital phase mask.

Also, in the interference between two different wavefronts, such as a plane wavefront and a spherical wavefront, the phase introduced by the illuminating wave or the reference wave can never be physically compensated. To obtain the correct object phase, numerical compensation is needed.

It seems that the presented method works well only for physical compensation of the spherical phase aberration. Actually, all kinds of aberrations may exist in a complicated optical setup. They may come from using elements with bad quality or from misalignment of all the optical elements used. The simpler the optical setup is, the less aberration will be introduced in the interference wavefront. The presented method is based on the Michelson interferometric configuration; thus the alignment of all the elements can be well ensured. This can be done by real-time monitoring of the spatial frequency spectra since aberrations other than spherical aberration will lead to defects in the spatial frequency spectrum of the recorded hologram.

6. CONCLUSION

In DHM, whatever the illumination wavefront used, the object phase will be introduced in the spherical phase, which can be physically compensated by a spherical reference wavefront. There is a determination that the Fourier spectra of the recorded digital hologram are pointlike

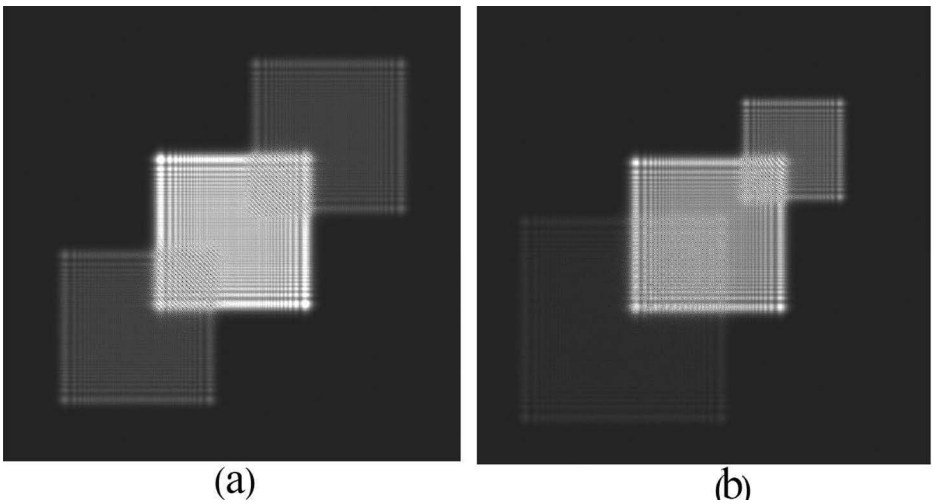

Fig. 7. Fourier spectra of holograms when the numerical spherical reference wave is used to illuminate the holograms. (a) Fourier spectra of the hologram in Fig. 2(a). (b) Fourier spectra of the hologram in Fig. 2(c).

spectra in the frequency domain. DHM setups based on the Michelson interferometric configuration with MO and an adjustable lens can well perform the quasi-physical compensation. The numerical reconstruction of a digital hologram can be easily accomplished without complicated numerical phase compensation. Simplicity in hardware and time-saving process in software will ensure DHM wide application in real-time monitoring and inspection.

ACKNOWLEDGMENT

This study is supported by Innovation Fund grant MOE2008-IF-1-009 from the Ministry of Education, Singapore.

REFERENCES

1. W. S. Haddad, D. Cullen, J. C. Solem, J. W. Longworth, A. McPherson, K. Boyer, and C. K. Rhodes, "Fourier-transform holographic microscope," Appl. Opt. **31**, 4973–4978 (1992).
2. U. Schnars and W. P. O. Jüptner, "Digital recording and numerical reconstruction of holograms," Meas. Sci. Technol. **13**, R85–R101 (2002).
3. F. Dubois, L. Joannes, and J. Legros, "Improved three-dimensional imaging with a digital holography microscope with a source of partial spatial coherence," Appl. Opt. **38**, 7085–7094 (1999).
4. C. Mann, L. Yu, C.-M. Lo, and M. Kim, "High-resolution quantitative phase-contrast microscopy by digital holography," Opt. Express **13**, 8693–8698 (2005).
5. T. Colomb, E. Cuche, F. Charrière, J. Kühn, N. Aspert, F. Montfort, P. Marquet, and C. Depeursinge, "Automatic procedure for aberration compensation in digital holographic microscopy and applications to specimen shape compensation," Appl. Opt. **45**, 851–863 (2006).
6. P. Marquet, B. Rappaz, P. J. Magistretti, E. Cuche, Y. Emery, T. Colomb, and C. Depeursinge, "Digital holographic microscopy: a noninvasive contrast imaging technique allowing quantitative visualization of living cells with subwavelength axial accuracy," Opt. Lett. **30**, 468–470 (2005).
7. B. Rappaz, P. Marquet, E. Cuche, Y. Emery, C. Depeursinge, and P. J. Magistretti, "Measurement of the integral refractive index and dynamic cell morphometry of living cells with digital holographic microscopy," Opt. Express **13**, 9361–9373 (2006).
8. E. Cuche, P. Marquet, and C. Depeursinge, "Simultaneous amplitude-contrast and quantitative phase-contrast microscopy by numerical reconstruction of Fresnel off-axis holograms," Appl. Opt. **38**, 6994–7001 (1999).
9. P. Ferraro, S. D. Nicola, A. Finizio, G. Coppola, S. Grilli, C. Magro, and G. Pierattini, "Compensation of the inherent wave front curvature in digital holographic coherent microscopy for quantitative phase-contrast imaging," Appl. Opt. **42**, 1938–1946 (2003).
10. T. Colomb, J. Kühn, F. Charrière, C. Depeursinge, P. Marquet, and N. Aspert, "Total aberrations compensation in digital holographic microscopy with a reference conjugated hologram," Opt. Express **14**, 4300–4306 (2006).
11. T. Colomb, F. Montfort, J. Kühn, N. Aspert, E. Cuche, A. Marian, F. Charrière, S. Bourquin, P. Marquet, and C. Depeursinge, "Numerical parametric lens for shifting, magnification, and complete aberration compensation in digital holographic microscopy," J. Opt. Soc. Am. A **23**, 3177–3190 (2006).
12. F. Montfort, F. Charrière, T. Colomb, E. Cuche, P. Marquet, and C. Depeursinge, "Purely numerical compensation for microscope objective phase curvature in digital holographic microscopy: influence of digital phase mask position," J. Opt. Soc. Am. A **23**, 2944–2953 (2006).
13. Z. Ya'nan, Q. Weijuan, L. De'an, L. Zhu, Z. Yu, and L. Liren, "Ridge-shape phase distribution adjacent to 180° domain wall in congruent $LiNbO_3$ crystal," Appl. Phys. Lett. **89**, 112912-1–3 (2006).
14. D. Malacara, ed. *Optical Shop Testing*, 3rd ed. (Wiley, 2007).
15. T. Colomb, P. Marquet, F. Charrière, J. Kühn, P. Jourdain, B. Rappaz, P. Magistretti, and C. Depeursinge, "Enhancing the performance of digital holographic microscopy," in *SPIE Newsroom* 10.1117/2.1200709.0872 (2007).
16. E. Cuche, P. Marquet, and C. Depeursinge, "Spatial filtering for zero-order and twin-image elimination in digital off-axis holography," Appl. Opt. **39**, 4070–4075 (2000).